ISSN: 2160-049X Volume 9, Number 4, April 2019

Scientific Research Publishing

World Journal of Mechanics

ISSN: 2160-049X
9 772160 049007 04

www.scirp.org/journal/wjm

Journal Editorial Board

ISSN 2160-049X (Print) ISSN 2160-0503 (Online)

http://www.scirp.org/journal/wjm

Editors-in-Chief

Scientific Research Publishing

World Journal of Mechanics, 2019, 9, 67-93
http://www.scirp.org/journal/wjm
ISSN Online: 2160-0503
ISSN Print: 2160-049X

Table of Contents

Volume 9 Number 4 April 2019

World Journal of Mechanics (WJM)
Journal Information

SUBSCRIPTIONS

The *World Journal of Mechanics* (Online at Scientific Research Publishing, www.SciRP.org) is published monthly by Scientific Research Publishing, Inc., USA.

Subscription rates:
Print: $69 per issue.
To subscribe, please contact Journals Subscriptions Department, E-mail: sub@scirp.org

SERVICES

Advertisements
Advertisement Sales Department, E-mail: service@scirp.org

Reprints (minimum quantity 100 copies)
Reprints Co-ordinator, Scientific Research Publishing, Inc., USA.
E-mail: sub@scirp.org

COPYRIGHT

PRODUCTION INFORMATION

For manuscripts that have been accepted for publication, please contact:
E-mail: wjm@scirp.org

World Journal of Mechanics, 2019, 9, 67-80
http://www.scirp.org/journal/wjm
ISSN Online: 2160-0503
ISSN Print: 2160-049X

Existence of Chaotic Phenomena in a Single-Well Duffing Oscillator under Parametric Excitations

Everestus Obinwanne Eze[1], Okorafor Chinenye Goodluck[1], Ujumadu Rosary Ngozi[2], Toochukwu Ogbonnia Oko[1]

[1]Department of Mathematics, Michael Okpara University of Agriculture, Umudike, Nigeria
[2]Department of Mathematics, Chukwuemeka Odimegwu Ojukwu University, Uli, Nigeria
Email: obinwanneeze@gmail.com, rozyngujumadu@yahoo.com, Okoraforchinenye11@gmail.com, tochukwu183@gmail.com

How to cite this paper: Eze, E.O., Goodluck, O.C., Ngozi, U.R. and Oko, T.O. (2019) Existence of Chaotic Phenomena in a Single-Well Duffing Oscillator under Parametric Excitations. *World Journal of Mechanics*, **9**, 67-80.
https://doi.org/10.4236/wjm.2019.94005

Received: November 16, 2018
Accepted: April 22, 2019
Published: April 25, 2019

Abstract

In this paper, the existence of chaotic behavior in the single-well Duffing Oscillator was examined under parametric excitations using Melnikov method and Lyapunov exponents. The minimum and maximum values were obtained and the dynamical behaviors showed the intersections of manifold which was illustrated using the MATCAD software. This extends some results in the literature. Simulation results indicate that the single-well oscillator is sensitive to sinusoidal signals in high frequency cases and with high damping factor, the amplitude of the oscillator was reduced.

Keywords

Single-Well Duffing Oscillator, Melnikov Method, Positive Lyapunov Exponent, Threshold Values, MATCAD Software

1. Introduction

Duffing oscillators have received remarkable attention in the recent decades due to the variety of their Engineering applications, for example magneto-elastic mechanical system [1], large amplitude oscillator of centrifugal governing system [2], nonlinear vibration beans and plates [3] [4] and fluid flow induced vibration [5]. It is famous for the existence of chaos behavior in recent decades [6]. In 1979, the chaotic phenomena in Duffing equation had been investigated by Ueda [7]. Chaos occurs when the behavior of the dynamical system is extremely sensitive to initial conditions. In mechanical system, it means a motion which trajectories starting from slightly different initial conditions diverge exponen-

tially.

Various researchers have used different methods in obtaining solutions, for instance, Ueda [7] used the numerical simulation where changes in attractors were obtained under various parameters.

The problem in Duffing-type system still remains a puzzle to so many scientists for instance, suppressing and inducing of chaos, influence of time delay, fractional dynamics [8]-[13].

Melnikov method and Lyapunov exponents are very significant analytical techniques for determining chaos. The main idea of this method is to measure the distance between the stable and unstable manifolds and if the stable and unstable manifolds intensively intersect once, they will intersect infinite times [6]. Thus, according to Smale-Birkhoff theorem in [1], it implies the existence of the chaotic behavior in the Smale-horseshoe sense. The Melnikov theory was firstly used to study chaos in Duffing system by Holmes [2] and generalized Melnikov function was developed by Wiggins [13] [14]. This criterion is just the necessary condition for chaos but not sufficient for chaos, therefore, it must be sufficient conditions for the suppression of chaos [15]. The Lyapunov exponent is an important indicator in determining the sensitivity of chaotic behavior which characterizes the average rate of the system in phase space between adjacent tracks of convergence and divergence [16]. Whether the Lyapunov exponent is greater than zero or not is one of the most straight forward criterions to distinguish the chaotic systems [17]. In other to calculate the Lyapunov exponent, some methods of solutions includes [16], nonlinear adaptive filtering method, QR matrix factorization method and its improvement methods. This paper makes use of two methods, the Melnikov method and improved QR matrix factorization.

The objectives of this paper therefore are to investigate the existence of chaotic behavior in a single-well Duffing oscillator forced by parametric excitations.

The rest of the paper is organized as follows: Section 2, explained the preliminaries to the results, Section 3 gives the main results using the Melnikov method and the calculation of the Lyapunov exponent and Section 4 presents the numerical simulations and finally some conclusions are given in Section 5.

2. Preliminaries

2.1. Melnikov Method

One of the main tools for determining the existence or non-existence of chaos in a perturbed Hamiltonian system is Melnikov. In his theory, the distance between stable and unstable manifolds of the perturbed system were calculated up to the first order term.

Melnikov method is a procedure which gives a bound on the parameters of a system such that chaos is predicted not to occur. The Melnikov method investigate the homoclinic bifurcation in the forced Duffing oscillator system with linear and non-damping. It measures the distance between stable and unstable manifolds in the Poincare section [6] and to preserve the homoclinic loops un-

der a perturbation requires that at t_0, if $M(t_0)$, that is the Melnikov function has a simple zero, then a homoclinic bifurcation occurs, implying that the chaotic motion occurs.

2.2. Melnikov Method for Predicting Chaos

Melnikov method gives an analytic tool for establishing the existence of transverse homoclinic points of the Poincare map for a periodic orbit of a perturbed dynamical system of the form;

$$\dot{x} = f(x) + \varepsilon g(x). \tag{1}$$

with $x \in R^n$. It can also be used to establish the existence of sub-harmonic periodic orbits of perturbed system of the form in (1). Furthermore, it can be used to show the existence of limit cycles and separatix cycles of perturbed planar system with $x \in R^2$. For periodically perturbed planar systems, we have the form;

$$\dot{x} = f(x) + \varepsilon g(x,t). \tag{2}$$

where $x \in R^2$ and g is periodic with period t in T. We assume that $f \in C'(R^2)$ and $g \in C'(R^2 \times R)$ and we make the assumption;

1) For $\varepsilon = 0$, the system (2) has a homoclinic orbit;

$\Gamma_0 : \boldsymbol{X} = \gamma_0(t), -\infty < t < \infty$ at a hyperbolic saddle point $\boldsymbol{X}_0$ and

2) For $\varepsilon = 0$, the system has a non-parametric family of periodic orbit. Then the Melnikov function $M(t_0)$ is defined as;

$$M(t_0) = \int_{-\infty}^{\infty} f(\gamma_0(t)) \wedge g(\gamma_0(t), t + t_0) \mathrm{d}t. \tag{3}$$

The Melnikov method can be interpreted as a derivation in energy from the value on the perturbed separatix. Before stating main result established by Melnikov concerning the existence of transverse homoclinic point of the Poincare section, we need the following lemma and theory which establish the existence of a periodic orbit and hence the existence of the Poincare map with sufficient ε.

Lemma 2.1

Under assumption 1) and 2), for ε sufficiently small, the system (2) has a unique hyperbolic periodic orbit; $\gamma_\varepsilon(t) = X_0 + 0_{(\varepsilon)}$ of period T. Correspondingly, the Poincare map P_ε has a unique hyperbolic fixed point of saddle type;

$$X_\varepsilon = X_0 + 0_{(\varepsilon)}. \tag{4}$$

Theorem 2.1

Under the assumption 1) and 2), if the Melnikov function $M(t_0)$ has a simple zero in [0,1], then for all sufficiently small $\varepsilon \neq 0$, the stable and unstable manifold of the Poincare map P_ε intersect transversally, that is, P_ε has a transverse homoclinic point.

This theorem was established by Melnikov [1]. The idea of the proof is that $M(t_0)$ is a measure of the separation of the stable and unstable manifold of the Poincare map. The theory is an important result because it establishes the existence of transverse homoclinic point for P_ε. It implies the existence of strange

invariant set for some iterate of P_ε and the same type of chaotic dynamics for system (2) as for the Smale horseshoe map. Generally, the Melnikov method is very useful for detecting the presence of transverse homoclinic orbits and the occurance of homoclinic bifurcations.

Theorem 2.2 (Smale-Birkhoff Homoclinic Theorem) [18]

Let f be a diffeomorphism (C') and suppose p is a hyperbolic fixed point. A homoclinic point is a point $q \neq p$ which is in the stable and unstable manifolds. If the stable and unstable manifolds intersect transversally at q, then q is called transverse. This implies that there is a homoclinic orbit $\gamma(q) = q_n$ such that $\lim_{n\to\infty} q_n = \lim_{n\to\infty} q_n = p$. Since the stable and unstable manifolds are invariant, we have; $q_n \in W^s(p) \cap W^u(p)$ for all $n \in \mathbb{Z}$. Moreover, if q is transversal, so are all q_n since f is diffeomorphism.

2.3. Method of Lyapunov Exponent

The method of Lyapunov exponent serves as a useful tool to qualify chaos. Specifically, Lyapunov exponent measures the rate of convergence or divergence of nearby trajectories [16] [18]. Negative Lyapunov exponents indicate convergence while positive Lyapunov exponents demonstrate divergence and chaos. The magnitude of the Lyapunov exponents is an indicator of the time scale on which chaotic behavior can be predicted or transients for the positive and negative cases respectively [19].

Physically, the Lyapunov exponent measures average exponential divergence or convergence between trajectories that differ only in having an infinitesimally small difference in their initial condition. The system is said to be chaotic if the trajectories remain within a bounded set of the dynamics. If one considers a ball of points in N-dimensional phase space in which each point follows its own trajectory based upon the system equations of motion over time, the ball of points will collapse to a simple point, will stay a ball or will become ellipsoid in shape [20]. The measure of the rate at which this infinitesimal ball collapse or expands is the Lyapunov exponent. For a system written in the state-space form $\dot{x} = u(x)$, small derivation from trajectory can be expressed by the equation $\delta\dot{x}_i = \frac{\partial u_i}{\partial x_j}\delta x_j$. The maximal Lyapunov exponent is then defined by this equation.

Other useful quantities are the short time Lyapunov exponent and the local Lyapunov exponent. A short time Lyapunov exponent is simply a Lyapunov exponent defined over some finite time interval. The local Lyapunov exponent is a short time Lyapunov exponent in the limit where the time interval approaches zero. Both are dependent on starting points and the short time Lyapunov exponent is also independent on the magnitude of the time interval. If all points in the neighborhood of a trajectory converge towards the same orbit, the attractor is a fixed point or a limit cycle. However, if the attractor is strange, any two trajectories $x(t) = f'(x_0)$ and $x(t) + \delta x(t) = f'(x_0 + \delta x_0)$ that starts over very close to each other separate exponentially with time. This sensitive initial condition can be quantified as;

$$\left\|\delta x(t)\right\| = \mathrm{e}^{\lambda t}\left\|\delta x_0\right\| \tag{5}$$

where λ, the mean rate of separation of trajectories of the system is called the Lyapunov exponent, which can be estimated for long time t as;

$$\lambda = \frac{1}{t}\ln\frac{\left\|\delta x(t)\right\|}{\left\|\delta x_0\right\|} \tag{6}$$

$$\lambda_T\left(X(t),\delta x_0\right) = \frac{1}{T}\ln\frac{\left\|\delta X(t+T)\right\|}{\left\|\delta x(t)\right\|} \tag{7}$$

$$\lambda_{local}\left(X(t)\right) = \lim\frac{1}{T}\ln\frac{\left\|\delta X(t+T)\right\|}{\left\|\delta X(t)\right\|} \tag{8}$$

Equations (7) and (8) are for short and local Lyapunov exponent. The exponent can be positive or negative but at least one must be positive for an attractor to be classified as chaotic. In particular, if $\lambda < 0$, the system converges to a stable fixed point or periodic orbits. A negative value of the Lyapunov exponent is characteristic of dissipative or non-conservative systems. If $\lambda = 0$, the system is conservative and converges to a stable cycle limit. If $\lambda > 0$, the system is unstable and chaotic. Hence, if the system is chaotic, it will have at least one positive Lyapunov exponent. Thus, the definition of chaotic system is based on a positive Lyapunov exponent. Finally, If $\lambda = \infty$, the system is random.

Generally, the most used measure of sensitive initial condition is a system characterization by the Lyapunov exponent, which quantifies the rate of separation of infinitesimal close trajectories. For example, consider a one-dimensional system with two trajectories $x_1(t)$ and $x_2(t)$ which at some point t_0 are arbitrary close together and their difference in time tracked by the function; $\delta x(t) = \left|x_1(t) - x_2(t)\right|$. The sign of the lyapunov exponent characterizes whether or not the system is exhibiting chaotic behavior. If the exponent is negative, the system, at least in that set of initial conditions is said to be stable (like trajectories go to like trajectories). A Lyapunov exponent of zero implies an unstable system which is essentially on the edge stable and chaotic. And of course a positive exponent implies the system is chaotic where trajectories exhibit exponential divergence.

3. Results

3.1. The Single-Well Duffing Oscillator

The single-well Duffing equation under parametrical excitation is shown below;

$$\ddot{x} + \varepsilon k\dot{x} + \alpha x + \beta x^3 = \varepsilon\gamma\cos(\omega t) \tag{9}$$

The System (9) has a unique hyperbolic limit cycle. Using the Melnikov theory, an analysis has been performed of the limit circles in oscillator systems described by single-well Duffing equation under perturbation.

Briefly, we describe Melnikov function and the bifurcations in perturbed Hamiltonian system as;

$$\left.\begin{aligned}\dot{x} &= \frac{\partial H}{\partial y} + \varepsilon p(x,y)\\ \dot{y} &= \frac{\partial H}{\partial x} + \varepsilon q(x,y)\end{aligned}\right\} \tag{10}$$

where H the Hamiltonian $H = H(x,y)$ is the analytic function. Also the perturbation functions $p(x,y)$ and $q(x,y)$ are analytic, ε is a small parameter.

Let $(x,y) = x_\varepsilon(t), y_\varepsilon(t)$ be the solution of (3.1). Then the solution of the unperturbed system at ($\varepsilon = 0$) is $(x,y) = (x_0(t), y_0(t))$. Further, we note that the unperturbed system at $\varepsilon = 0$ has one equilibrium point *i.e.* the center surrounded by a closed trajectories.

3.2. Melnikov Function for the Perturbed Single-Well Duffing Equation

In this work, the single-well Duffing equation is represented by;

$$\ddot{x} + \varepsilon k\dot{x} + \alpha x + \beta x^3 = \varepsilon\gamma\cos(\omega t)$$

This equation can be rewritten in the following perturbed Hamiltonian system;

$$\left.\begin{aligned}\dot{x} &= y + \varepsilon(ky + \gamma\cos\omega t)\\ \dot{y} &= -\alpha x - \beta x^3\end{aligned}\right\} \tag{11}$$

where $\alpha, \beta > 0$.

Let $(x,y) = x_\varepsilon(t), y_\varepsilon(t)$ be the solution of (11). The unperturbed system (11) has a Hamiltonian;

$$H = \frac{1}{2}y^2 + \frac{\alpha}{2}x^2 + \frac{\beta}{4}x^4. \tag{12}$$

and one equilibrium point surrounded by a closed trajectories.

The solution of the unperturbed system is expressed as;

$$x_0(t) = \frac{\sqrt{2}\sqrt{ak}\sqrt{1-k^2}}{\sqrt{b}\sqrt{1-2k^2}}\, sd\left(\frac{\sqrt{a}}{\sqrt{1-2k^2}}t, k\right). \tag{13}$$

where *sd* is a Jacobian function.

Then, the Melnikov function for the System (3) is given as;

$$\begin{aligned}M(t_0) &= \int_0^{T_0}(-kx_0(t) + \gamma\cos\omega t)\,\mathrm{d}t\\ &= \int_0^{T_0} -kx_0(t)\,\mathrm{d}t + \int_0^{T_0}\gamma\cos\omega t\,\mathrm{d}t\\ &= -kL_1 + \gamma L_2\end{aligned} \tag{14}$$

now taking (13) into (14), we get;

$$\begin{aligned}L_1 &= \int_0^{T_0} x_0(t)\,\mathrm{d}t\\ &= \int_0^{T_0}\frac{\sqrt{2}\sqrt{ak}\sqrt{1-k^2}}{\sqrt{b}\sqrt{1-2k^2}}\, sd\left(\frac{\sqrt{a}}{\sqrt{1-2k^2}}t, k\right)\end{aligned} \tag{15}$$

Then, using the following properties;

$$T_0 = 4k\left(k^2\right)\frac{\sqrt{1-2k^2}}{\sqrt{a}} \tag{A3}$$

$$Sd\left(z,k\right) = 0 \tag{A2}$$

$$\int_0^{4k} sd^{2n}\left(z,k\right)\mathrm{d}z = 4\int_0^{k} sd^{2n}\left(z,k\right)\mathrm{d}z \tag{A3}$$

The Melnikov function becomes;

$$M\left(t_0\right) = \frac{4\sqrt{1-2k^2}}{\sqrt{a}}\left[\int_0^{k}\frac{\sqrt{2}\sqrt{ak}\sqrt{1-k^2}}{\sqrt{b}\sqrt{1-2k^2}}sd^{2n}\left(z,k\right)\right]\mathrm{d}z \tag{16}$$

after a long calculation and introducing the notation $m = k^2$ and the following identities;

$$\int_0^{k} sd^2\mathrm{d}z = \frac{1}{k^2\left(1-k^2\right)}$$

$$\int_0^{k} sd^4\mathrm{d}z = \frac{1}{3k^4\left(1-k^2\right)}$$

We obtain the final expression as;

$$M\left(t_0\right) = \frac{8\lambda\sqrt{a}\sqrt{1-2m}}{\left(1-2m\right)^2}$$

where $\lambda = a/b$.

3.3. The Lyapunov Exponent of a Single-Well Duffing Oscillator

Consider the Duffing equation below;

$$\ddot{x} + k\dot{x} + \alpha x + \beta x^3 = \gamma\cos\left(\omega t\right) \tag{17}$$

where $\ddot{x}$ and $\dot{x}$ are second-order and first-order derivative, $\alpha \in \mathcal{R}^n$, $\beta \in \mathcal{R}^n$, δ is the damping, γ is the amplitude of the circle, ω is the angular frequency of the driven circle. In other to Type equation here, determine whether the system is in chaotic state, we need to calculate the Lyapunov exponent using the QR factorization method.

Let $y = \dot{x}$, $g\left(x,y\right) = -ky - \alpha x - \beta x^3$

Then Equation (1) is equivalent to;

$$\left.\begin{aligned}\dot{x} &= y\\ \dot{y} &= g\left(x,y\right) + f\left(t\right)\end{aligned}\right\} \tag{18}$$

which is written in matrix form as;

$$\dot{Y}\left(x\right) = F\left(Y\right) \tag{19}$$

According to the variational principle, its variational equations are;

$$\dot{Y}\left(t\right) = J\left(t\right)Y\left(t\right),\ Y\left(0\right) = I \tag{20}$$

where $Y\left(t\right)$ is a 2 by 2 matrix, I is a 2 by 2 unit matrix, $J\left(t\right)$ is the Jacobian matrix of the system and its expression is;

$$\begin{pmatrix} \frac{\partial f}{\partial x} & \frac{\partial f}{\partial y} \\ \frac{\partial g}{\partial x} & \frac{\partial g}{\partial y} \end{pmatrix} = \begin{pmatrix} 0 & 1 \\ -\alpha - 3\beta x^2 & -k \end{pmatrix}$$

Then, QR factorization of $Y(t)$ can be written as;

$$Y(t) = QR \tag{21}$$

where Q is orthogonal matrix, R is upper triangular matrix. Substituting (21) in (20), we obtain the variational equation;

$$\dot{Q}R + Q\dot{R} = JQR. \tag{22}$$

$$Q(0)R(0) = I$$

Left multiply Equation (22) by Q^{T} and right multiply by R^{-1}, we have;

$$Q^{\mathrm{T}}\dot{Q} + \dot{R}R^{-1} = Q^{\mathrm{T}}JQ \tag{23}$$

$$Q(0) = I, R(0) = I$$

The orthogonal matrix Q is written as a function of angle variables. To the Duffing equation, its orthogonal matrix Q can be expressed by one angle θ.

$$Q = \begin{bmatrix} \cos\theta & \sin\theta \\ -\sin\theta & \cos\theta \end{bmatrix}$$

The upper triangular matrix R can be expressed as;

$$R = \begin{bmatrix} \mathrm{e}^{\lambda_1(t)} & r_{12} \\ 0 & \mathrm{e}^{\lambda_2(t)} \end{bmatrix}$$

where θ is the angle variable, $\lambda_i(t)$ is the value associated with the Lyapunov exponent. Then,

$$Q^{\mathrm{T}} = \begin{bmatrix} \cos\theta & -\sin\theta \\ \sin\theta & \cos\theta \end{bmatrix}$$

$$R^{-1} = \begin{bmatrix} \mathrm{e}^{-\lambda_1(t)} & \frac{-r_{12}}{\mathrm{e}^{\lambda_1+\lambda_2}} \\ 0 & \mathrm{e}^{-\lambda_2(t)} \end{bmatrix}$$

Then putting $Q^{\mathrm{T}}, R^{-1}, Q$ and R into Equation (23), we have;

$$\begin{bmatrix} \cos\theta & -\sin\theta \\ \sin\theta & \cos\theta \end{bmatrix}\begin{bmatrix} -\sin\theta & \cos\theta \\ -\cos\theta & -\sin\theta \end{bmatrix} + \begin{bmatrix} \frac{\mathrm{d}\mathrm{e}^{\lambda_1(t)}}{\mathrm{d}t} & \frac{\mathrm{d}r_{12}}{\mathrm{d}t} \\ 0 & \frac{\mathrm{d}\mathrm{e}^{\lambda_2(t)}}{\mathrm{d}t} \end{bmatrix}\begin{bmatrix} \mathrm{e}^{-\lambda_1(t)} & \frac{-r_{12}}{\mathrm{e}^{\lambda_1+\lambda_2}} \\ 0 & \mathrm{e}^{-\lambda_2(t)} \end{bmatrix}$$

$$= \begin{bmatrix} \cos\theta & -\sin\theta \\ \sin\theta & \cos\theta \end{bmatrix}\begin{bmatrix} 0 & 1 \\ -\alpha - 3\beta x^2 & -k \end{bmatrix}\begin{bmatrix} \cos\theta & \sin\theta \\ -\sin\theta & \cos\theta \end{bmatrix}$$

The correspondent matrix elements on both sides of (23) are equal, so we get;

$$\left.\begin{aligned}\frac{\mathrm{d}\lambda_1(t)}{\mathrm{d}t} &= \frac{\partial g}{\partial y}\sin^2\theta - \frac{1}{2}\left[1+\frac{\partial g}{\partial x}\right]\sin(2\theta)\\ \frac{\mathrm{d}\lambda_2(t)}{\mathrm{d}t} &= \frac{\partial g}{\partial y}\cos^2\theta + \frac{1}{2}\left[1+\frac{\partial g}{\partial x}\right]\sin(2\theta)\\ \frac{\mathrm{d}\theta(t)}{\mathrm{d}t} &= -\frac{1}{2}\frac{\partial g}{\partial y}\sin 2\theta + \sin^2\theta - \frac{\partial g}{\partial x}\cos^2\theta\end{aligned}\right\} \tag{24}$$

We add and subtract the first two differential equations and get a new differential equation. Together with the third differential equation, we obtain three new equations;

$$\left.\begin{aligned}\frac{\mathrm{d}v_1}{\mathrm{d}t} &= \frac{\partial g}{\partial y}\\ \frac{\mathrm{d}v_2}{\mathrm{d}t} &= \frac{\partial g}{\partial y}\cos 2\theta - \frac{1}{2}\left[1+\frac{\partial g}{\partial x}\right]\sin(2\theta)\\ \frac{\mathrm{d}\theta(t)}{\mathrm{d}t} &= -\frac{1}{2}\frac{\partial g}{\partial y}\sin 2\theta + \sin^2\theta - \frac{\partial g}{\partial x}\cos^2\theta\end{aligned}\right\} \tag{25}$$

Then from;

$$\left.\begin{aligned}\frac{\mathrm{d}v_1}{\mathrm{d}t} &= \frac{\mathrm{d}\lambda_1}{\mathrm{d}t} + \frac{\mathrm{d}\lambda_2}{\mathrm{d}t}\\ \frac{\mathrm{d}v_2}{\mathrm{d}t} &= \frac{\mathrm{d}\lambda_1}{\mathrm{d}t} - \frac{\mathrm{d}\lambda_2}{\mathrm{d}t}\end{aligned}\right\} \tag{26}$$

We obtain;

$$\left.\begin{aligned}\lambda_1(t) &= \frac{\left[v_1(t)+v_2(t)\right]}{2}\\ \lambda_2(t) &= \frac{\left[v_1(t)-v_2(t)\right]}{2}\end{aligned}\right\} \tag{27}$$

The time evolution of the Lyapunov exponent is;

$$\left.\begin{aligned}f_1(t) &= \frac{\lambda_1(t)}{t}\\ f_2(t) &= \frac{\lambda_2(t)}{t}\end{aligned}\right\} \tag{28}$$

Then, the Lyapunov exponent is;

$$\left.\begin{aligned}\lambda_1 &= \lim_{t\to\infty}\frac{\lambda_1(t)}{t}\\ \lambda_2 &= \lim_{t\to\infty}\frac{\lambda_2(t)}{t}\end{aligned}\right\} \tag{29}$$

4. Numerical Simulation of Single-Well Duffing Oscillator

In this section, we compare the numerical solution of Equation (9) using MATCAD simulation. In Figures 1-6, the trajectory versus time response curves are plotted for different sets of parameter values noted in the figure captions. In all figures, the solid lines represent the numerical solution and the dashed lines

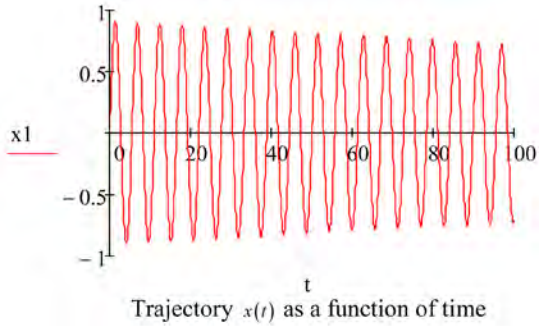

Figure 1. Trajectory-time response curves and parameter values of $\varepsilon = 0.01$, $\alpha = 1$, $\beta = 0.5$, $k = 0.5$, $\omega = 0.1$. The solid lines represent the numerical solution and the dash lines represent the chaotic behavior.

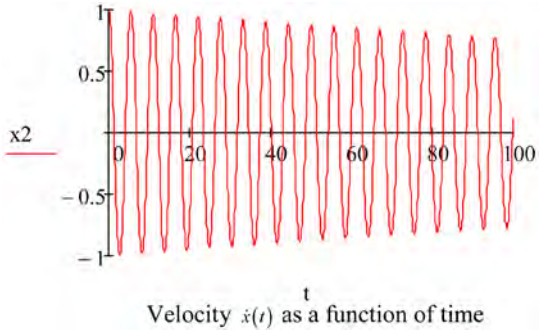

Figure 2. Velocity-time response curves and parameter values of $\varepsilon = 0.01$, $\alpha = 1$, $\beta = 0.5$, $k = 0.5$, $\omega = 0.1$. The solid lines represent the numerical solution and the dash lines represent the chaotic behavior.

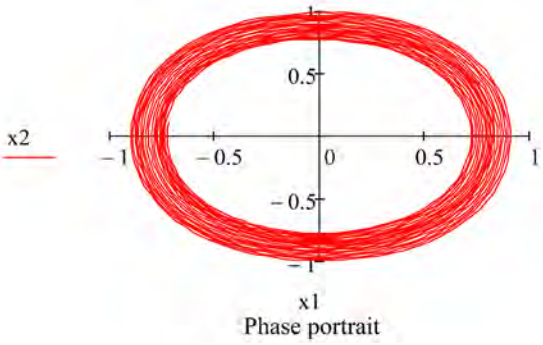

Figure 3. The phase portrait orbits in the chaotic state at $k = 0.5$. $\varepsilon = 0.01$, $\alpha = 1$, $\beta = 0.5$, $k = 0.5$, $\omega = 0.1$.

represent our chaotic solutions.

Figure 1 and Figure 2 compare solutions by considering a strong nonlinearity value of $\varepsilon = 0.01$. The periodic solution of the Duffing's equation were shown by the relationship between the first solution function values and the independent variables values as shown in Table 1. The values were generated using the vector initial function values and the constant. However, the solutions are in

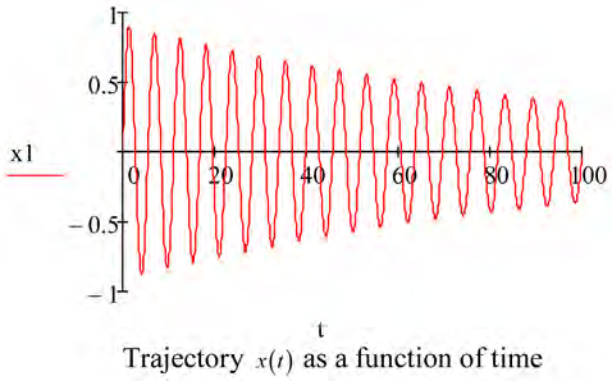

Figure 4. Trajectory-time response curves and parameter values of $\varepsilon = 0.01$, $\alpha = 1$, $\beta = 0.5$, $k = 0.5$, $\omega = 0.1$. The solid lines represent the numerical solution and the dash lines represent the chaotic behavior.

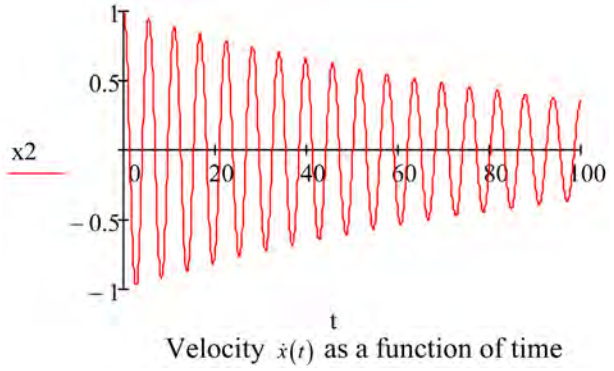

Figure 5. Velocity-time response curves and parameter values of $\varepsilon = 0.01$, $\alpha = 1$, $\beta = 0.5$, $k = 0.5$, $\omega = 0.1$. The solid lines represent the numerical solution and the dash lines represent the chaotic behavior.

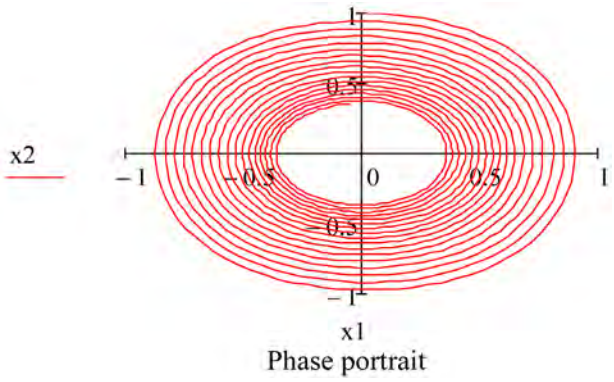

Figure 6. The phase portrait orbits in the chaotic state at $k = 2$.

good agreement over the time interval shown. Also, at $t = 0.067$, the maximum trajectory is $x = 0.998$. **Figure 3** is the phase diagram of the chaotic system at $\varepsilon = 0.01$ and damping factor $k = 1$.

The same conclusion can be drawn from Figures 4-6 but with damping factor at $k = 2$. The solutions are in excellent agreement over the time interval shown. However, Figure 6 is the phase portrait of the chaotic system.

$$\ddot{x} + \varepsilon k\dot{x} + ax + \beta x^3 = \varepsilon y \cos(\omega t)$$

$$\varepsilon := 0.01,\ a := 1,\ \beta := 0.5,\ k := 0.5,\ \omega := 0.1$$

Define a function that determines a vector of derivatives values at any solution point (t, Y):

$$D(t, X) := \begin{bmatrix} X_1 \\ \varepsilon \cdot y \cdot \cos(\omega \cdot t) - \varepsilon \cdot k \cdot X_1 - a \cdot X_0 - b \cdot (X_0)^3 \end{bmatrix}$$

Define an additional argument for the ODE solver:

$t_0 := 0$ Initial value of independent variable

$t_1 := 100$ Final value of independent variable

$X_0 := \begin{pmatrix} 0 \\ 1 \end{pmatrix}$ Vector of initial function values

$N := 1500$ Numbers of solution values on $[t_0, t_1]$

$$S := (X_0, t_0, t_1, N, D)$$

$t := S^{\langle 0 \rangle}$ Independent variables values

$X_1 := S^{\langle 1 \rangle}$ First solution function values

$X_2 := S^{\langle 2 \rangle}$ Second solution function values

Table 1. Solution matrix table for solution functions.

	0	1	2
0	0	0	0
1	0.067	0.067	0.998
2	0.133	0.133	0.991
3	0.2	0.199	0.98
4	0.267	0.264	0.964
5	0.333	0.327	0.944
6	0.4	0.389	0.918
7	0.467	0.449	0.888
8	0.533	0.508	0.853
9	0.6	0.563	0.812
10	0.667	0.616	0.766
12	0.8	0.711	0.658
13	0.867	0.753	0.596
14	0.933	0.79	0.53
15	1	0.823	…

5. Conclusions

In the present study, the chaotic behavior in single-well Duffing oscillator is investigated using Melnikov approach and Lyapunov exponent. The distance between the stable and unstable manifold of the nonlinear system is calculated by Melnikov approach. The Lyapunov exponent of the nonlinear system is evaluated by QR factorization to determine whether the chaotic phenomenon of the nonlinear system actually occurs.

As a result, threshold values were obtained and the dynamical behaviors showing the intersections of manifold were illustrated. To detect the chaotic phenomena of the nonlinear system, the Melnikov approach, Lyapunov exponent, the time history, phase portrait of the nonlinear system were presented for various cases.

Conflicts of Interest

The authors declare no conflicts of interest regarding the publication of this paper.

References

[1] Guckenheimer, J. and Holmes, P. (1983) Global Bifurcations. In: *Nonlinear Oscillations, Dynamical Systems, and Bifurcations of Vector Fields*, Springer, New York, 289-352. https://doi.org/10.1007/978-1-4612-1140-2_6

[2] Holmes, P.J. (1979) A Nonlinear Oscillator with a Strange Attractor. *Philosophical Transaction of the Royal Society of London, Series A: Mathematical and Physical Science*, **292**, 419-448. https://doi.org/10.1098/rsta.1979.0068

[3] Kim, S. and Kim, Y. (2000) Dynamic Stabilization in the Double-Well Duffing Oscillator. *Physical Review*, **61**, 6517-6520. https://doi.org/10.1103/physreve.61.6517

[4] Venkatesan, A. and Lakshmanan, M. (1997) Bifurcation and Chaos in the Double-Well Duffing-van der Pol Oscillator: Numerical and Analytical Studies. *Physical Review*, **56**, 6321-6330. https://doi.org/10.1103/PhysRevE.56.6321

[5] McCue, L. and Troesch, A.W. (2011) Use of Lyapunov Exponents to Predict Chaotic Vessel Motions. In: Almeida Santos Neves, M., Belenky, V., de Kat, J., Spyrou, K. and Umeda, N., Eds., *Contemporary Ideas on Ship Stability and Capsizing in Waves*, Springer, Dordrecht, 415-432. https://doi.org/10.1007/978-94-007-1482-3_23

[6] Zhang, Y., Yue, X., Du, L., Wang, L. and Fang, T. (2016) Generation and Evolution of Chaos in Double-Well Duffing Oscillator under Parametrical Excitation. *Journal of Shock and Vibration*, **2016**, Article ID: 6109062. https://doi.org/10.1155/2016/6109062

[7] Ueda, Y. (1979) Randomly Transitional Phenomena in the System Governed by Duffing's Equation. *Journal of Statistical Physics*, **20**, 181-196. https://doi.org/10.1007/BF01011512

[8] Sun, Z.-K., Xu, W., Yang, X.-L. and Fang, T. (2006) Inducing or Suppressing Chaos in a Double-Well Duffing Oscillator by Time Delay Feedback. *Chaos, Solitons and Fractals*, **27**, 705-714. https://doi.org/10.1016/j.chaos.2005.04.041

[9] Liu, D., Li, J. and Xu, Y. (2014) Principle Resonance Responses of SDOF Systems with Small Fractional Derivative Damping under Narrow-Band Random Parametric

Excitation. *Communication in Nonlinear Science and Numerical Simulation*, **19**, 3642-3652. https://doi.org/10.1016/j.cnsns.2014.03.018

[10] Syta, A., Litak, G., Lenci, S. and Scheffler, M. (2014) Chaotic Vibrations of the Duffing System with Fractional Damping. *Chaos*, **24**, Article ID: 013107. https://doi.org/10.1063/1.4861942

[11] Tehrani, M.G., Wilmshurst, L. and Elliot, S.J. (2013) Reacceptance Method for Active Vibration Control of a Nonlinear System. *Journal of Sound and Vibration*, **332**, 4440-4449. https://doi.org/10.1016/j.jsv.2013.04.002

[12] Zhao, X.R., Xu, W., Yang, Y.G. and Wang, X.Y. (2016) Stochastic Responses of a Viscoelastic-Impact System under Additive and Multiplicative Random Excitations. *Communications in Nonlinear Science and Numerical Simulation*, **35**, 166-176. https://doi.org/10.1016/j.cnsns.2015.11.008

[13] Wiggins, S. (1988) Global Bifurcation and Chaos: Analytical Methods. Springer, New York. https://doi.org/10.1007/978-1-4612-1042-9

[14] Wiggins, S. (1990) Introduction to Applied Nonlinear Dynamical Systems and Chaos. Springer, New York. https://doi.org/10.1007/978-1-4757-4067-7

[15] Garcia-Margallo, J. and Bejarano, J.D. (1998) Melnikov's Method for Non-Linear Oscillators with Non-Linear Excitations. *Journal of Sound and Vibration*, **212**, 311-319. https://doi.org/10.1006/jsvi.1997.1443

[16] Wolf, A. (1986) Quantifying Chaos with Lyapunov Exponents. Chaos. Chapter, 13, Princeton University Press, Princeton, NJ. https://doi.org/10.1515/9781400858156.273

[17] Zeni, A.Z. and Gallas, A.C. (1995) Lyapunov Exponent for a Duffing Oscillator. *Physica D*: *Nonlinear Phenomena*, **89**, 71-82. https://doi.org/10.1016/0167-2789(95)00215-4

[18] Teschl, G. (2012) Ordinary Differential Equations and Dynamical Systems. American Mathematical Society, Providence, Rhode Island.

[19] Haken, H. (1981) Chaos and Order in Nature. *Proceedings of the International Symposium on Synergetics at Schloß Elmau*, Bavaria, Germany, April 27-May 2, 1981, 2-11. https://doi.org/10.1007/978-3-642-68304-6

[20] Glass, L. and Mackey, M.C. (1998) From Clock to Chaos: The Rhythms of Life. Princeton University Press, Princeton, NJ.

World Journal of Mechanics, 2019, 9, 81-93
http://www.scirp.org/journal/wjm
ISSN Online: 2160-0503
ISSN Print: 2160-049X

Hybrid Power Generation by Using Solar and Wind Energy: Case Study

Peter Jenkins[1], Monaem Elmnifi[2], Abdalfadel Younis[3], Alzaroog Emhamed[4]

[1]Department of Mechanical Engineering Department, University of Colorado, Denver, CO, USA
[2]Department of Mechanical Engineering, Bright Star University, Ajdabiya, Libya
[3]Department of Mechanical Engineering, Omar Al-Mukhtar University, Bayda, Libya
[4]Department of Electrical Engineering, Bright Star University, Ajdabiya, Libya
Email: Peter.jenkins@ucdenver.edu, Monm.hamad@yahoo.co.uk, Abdalfadel.younis@omu.edu.ly

How to cite this paper: Jenkins, P., Elmnifi, M., Younis, A. and Emhamed, A. (2019) Hybrid Power Generation by Using Solar and Wind Energy: Case Study. *World Journal of Mechanics*, **9**, 81-93.
https://doi.org/10.4236/wjm.2019.94006

Received: March 11, 2019
Accepted: April 25, 2019
Published: April 28, 2019

Abstract

Energy is critical to the economic growth and social development of any country. Indigenous energy resources need to be developed to the optimum level to minimize dependence on imported fuels, subject to resolving economic, environmental and social constraints. This led to an increase in research and development as well as investments in the renewable energy industry in search of ways to meet the energy demand and to reduce the dependency on fossil fuels. Wind and solar energy are becoming popular owing to the abundance, availability and ease of harnessing the energy for electrical power generation. This paper focuses on an integrated hybrid renewable energy system consisting of wind and solar energies. Many parts of Libya have the potential for the development of economic power generation, so maps locations were used to identify where both wind and solar potentials are high. The focal point of this paper is to describe and evaluate a wind-solar hybrid power generation system for a selected location. Grid-tied power generation systems make use of solar PV or wind turbines to produce electricity and supply the load by connecting to the grid. In this study, the HOMER (Hybrid Optimization Model for Electric Renewable) computer modeling software was used to model the power system, its physical behavior and its life cycle cost. Computer modeling software was used to model the power system, its physical behavior and its life cycle cost. The hybrid power system was designed for a building at the University of Al-Marj (MARJU). Through the use of simulations, the installation of ten 100-kW wind turbines and 150-KW solar PV was evaluated.

Keywords

Hybrid System, Solar and Wind Combination, Renewable Energy, Libya

1. Introduction

The main resources of energy usage in Libya are oil and gas which results in high emissions of carbon dioxides and other gases. The modern world emphasizes using renewable energy to generate electricity because of its low damage to the environment. The hybrid power plant is a newly developed technology that is used to convert solar energy combined with any system that generates energy [1] [2].

Since the oil crisis in the early 1970s, the utilization of the solar and wind power has increased significantly. In recent years, hybrid PV/wind systems have become viable alternatives to meet environmental protection requirements and electricity demands. A hybrid solar-wind energy system uses two renewable energy sources. Hence, efficiency and power reliability of the system increase. However, aggregating inherently stochastic power sources such as wind and solar to achieve reliable electricity supply is a non-trivial problem. To use solar and wind energy resources more efficiently and economically, the optimal sizing of hybrid PV/wind systems is important [3]. One of the applications of a PV array and wind turbine is constructing a hybrid energy system PV/wind for use in commercial buildings. The feasibility study of using hybrid energy systems has been an important subject of research around the world in recent years. For instance, Amutha and Rajini (2015) investigated the economic, technical and environmental performance of various hybrid power systems for powering a remote telecom [4]. They concluded that replacing the present arrangement of the diesel power telecom system with their proposed SPV/Wind or SPV/Wind/FC was not just economically justifiable, but also its environment-friendly nature makes it an attractive option to supplement the energy supply from other sources. Nafeh (2011) attempted to size an optimal PV-wind hybrid system by minimizing the total cost of the proposed hybrid energy system and maintaining the loss of power supply probability (LPSP) of the system less than a certain fixed value [5]. Dursun *et al*. (2013) investigated the possibility of obtaining electricity from solar/wind hybrid systems in the remote Turkish city of Edirne. He attempted to decrease the high cost of operating a standalone diesel system and achieve a substantial amount of fuel saving [6].

Ensuring energy security and energy resources used in this country in the future need to be diversified. Also, to ensure the continuity of supply, an energy mix needs to be rationalized by considering important factors, such as the economic cost, environmental impact, reliability of supplies and convenience to consumers. The hybrid renewable power generation is a system aimed at the production and utilization of the electrical energy stemming from more than one source, provided that at least one of them is renewable.

To evaluate the development of the wind-solar hybrid power generation systems in Libya solar energy and wind energy potentials are investigated at geographically locations by collecting data from different sources. Then, selected locations were analyzed using a software tool, the HOMER (Hybrid Optimization Model for Electric Renewable). This software is a micro-power optimization

model for both off-grid and grid connected power systems for a variety of applications. Wind-solar hybrid systems have numerous advantages [7] [8]. One of the advantages is reliability. When solar and wind power production resources are used together, the reliability is improved and the system energy service is enhanced. What this mean is that in the absence of one type of energy, another would be available to carry out the service. Other advantages are the stability and lower maintenance requirements; thus reducing downtime during repairs or routine maintenance. In addition, being indigenous and free, renewable energy resources contribute to the reduction of pollution emissions.

2. MARJU Hybrid Power Generation System

A design of a low cost power system that combines both wind electric and solar electric technologies is described in this paper. This hybrid system was designed to deliver 0.25 M Watts of continuous power to Al-Marj University (MARJU) to power a wide range of appliances and lower the consumption of the university that provided by the Libyan General Electric Company (Table 1). The system was composed of a wind generator, a solar panel, and an inverter. The solar panel and wind turbine work in tandem. An inverter was used to convert DC power into AC power suitable for domestic use.

3. Designing and Modeling of Hybrid System with HOMER

The Hybrid Optimization Model for Electric Renewable (HOMER), which is copyrighted by the Midwest Research Institute (MRI), is a computer model developed by the US National Renewable Energy Laboratory (NREL) to assist in the design of power systems and facilitate the comparison of power generation technologies across a wide range of applications (HOMER, ver.2.81 Beta).

Table 1. MARJU consumption [15].

Date	Total month consumption (MWH)	Average day consumption (MWH)	Consumption per hour (MWH)
Jan	57.6	1.92	0.240
Feb	51.52	1.84	0.230
Mar	50.40	1.68	0.210
Apr	46.8	1.56	0.195
May	47.56	1.64	0.205
Jun	56.40	1.88	0.235
Jul	57.6	1.92	0.240
Aug	58.8	1.96	0.245
Sep	50.4	1.68	0.210
Oct	54	1.8	0.225
Nov	60	2	0.250
Dec	57.6	1.92	0.240

HOMER is used to model a power systems physical behavior and its life-cycle cost, which is the total cost of installing and operating the system over its life time. HOMER performs three principal tasks: simulation, optimization and a sensitivity analysis based on the raw input data given by user. In the simulation process, the performance of a particular power system configuration for each hour of the year was modeled to determine its technical feasibility and lifecycle cost. HOMER can simulate a wide variety of power system configurations, comprising any combinations of PV array, wind turbines, run-off-river hydro turbines, generators and battery bank systems with grid connection or off-grid systems that can serve electrical and thermal loads. The simulation process serves two purposes. First, it determines whether the system is feasible. Second, it estimates the lifecycle cost of system, which is the total cost of installing and operating the system over its lifetime [9] [10].

3.1. Location Selection

The objective of the paper was to design and model a grid-connected wind-solar hybrid power generation system to meet a certain part of the load requirement of a local grid. As discussed in earlier, the Wind and Solar potential of different geographical locations were studied through literature searches and the detail analysis of identified locations (University of Al-Marj, Libya) was carried out as shown in Figure 1.

3.2. Wind and Solar Hybrid Power System Configuration

The grid connected wind solar hybrid system consisted of a local grid, PV arrays, wind turbines and inverters. The HOMER software was used as a tool to carry out the analysis. Figure 2 shows the configuration of the grid connected hybrid power system. HOMER requires input information in order to analyze a system. Those inputs are described in detail below.

3.2.1. Wind Resource

Hourly measured wind speed data from the NASA surface meteorology and solar energy database at 10 m height was used as the wind resource input data.

Figure 1. Geographical map of area (Proposed location for wind-solar hybrid power plant).

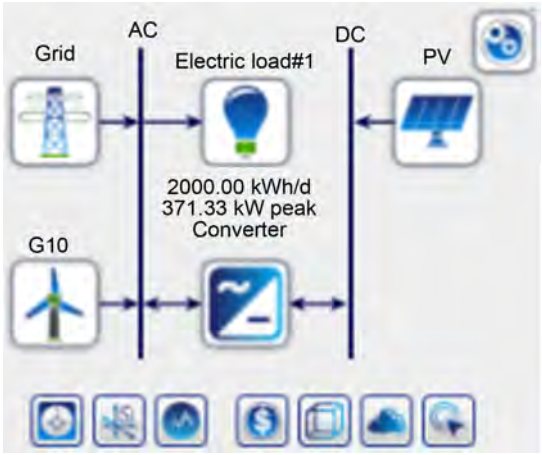

Figure 2. Configuration of grid connected hybrid wind-solar system in HOMER.

Figure 3 illustrates the monthly averaged wind speed data that was obtained. The average wind speed ranges from 4.4 m/s to 8.1 m/s with an annual average of 6.69 m/s.

3.2.2. Solar Radiation

The solar resource data gives the amount of global solar radiation that strikes earth surface in a typical year. The measured hourly average solar radiation on NASA surface meteorology and solar energy database was used as solar resource input data. The latitude was 32˚29' and the longitude was 20˚50' for this location. The average solar radiation ranges from 2.6 kWh/m^2/day to 7.9 kWh/m^2/day with an annual average of 5.4 kWh/m^2/day. The average clearness index is 0.56. The monthly average solar radiation and clearness index are shown in Figure 4 [11].

3.2.3. Wind Turbine

A wind turbine is a device that converts the kinetic energy of the wind into AC or DC electricity. Several wind turbine manufactures, such as Vestas, RE power, Gamesa, Siemens, GE Wind Energy, Enercon, etc. were evaluated for use in this model. The size of the turbine model to be used within a project was based on available wind turbine models, the wind resource at the site, and the ability to perform maintenance. The wind profile and wind speeds at each specific site were evaluated to identify which turbine was suitable for the particular site conditions. As the wind turbine itself may be as much as 70% of the total project cost it was vital that it produced the optimal electricity for the given site [12].

The most suitable wind turbine for the proposed plant was selected by considering wind power density, average wind speed and power requirement of the site. The wind turbine with a rated power of 150 kW was chosen for the design in order to harness the low wind speed efficiently. Figure 5 shows the power curve of the selected wind turbine, a Generic 10 KW. The Technical characteristics of Generic 10 KW are given in Table 2.

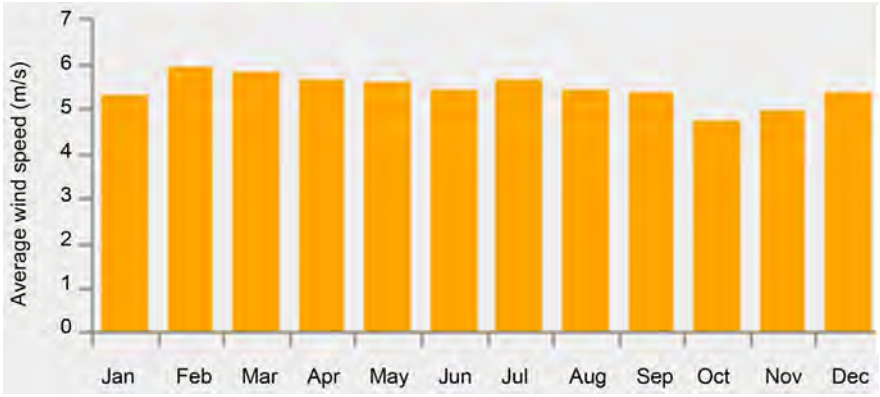

Figure 3. Monthly average wind speed data.

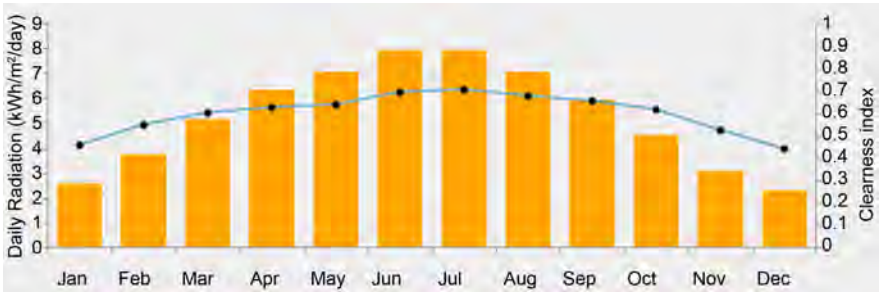

Figure 4. Monthly averaged solar radiation and clearness index.

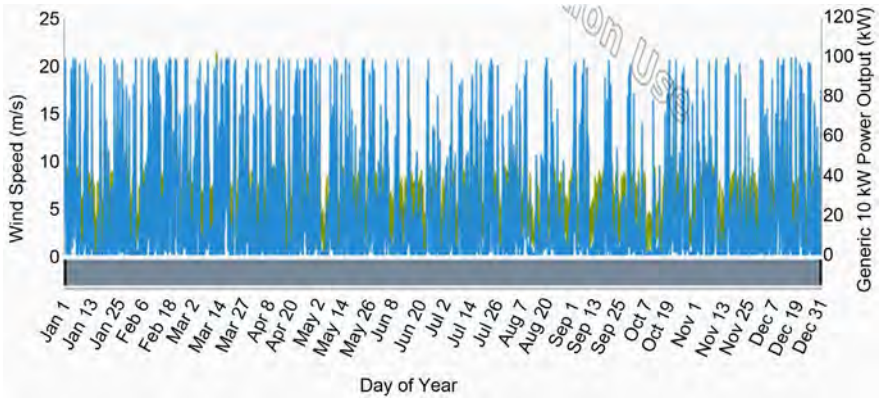

Figure 5. Power curve of generic 10 KW wind turbine.

Table 2. Generic 10 KW wind turbine specification.

Rated power	100 KW
Start up wind speed	3 m/s
Rated wind speed	12 m/s
Cut out wind speed	21 m/s
Tower height	50 m
Rotor diameter	22 m
Swept area	2300 m^2
Power regulation	Pitch regulated with variable speed

The installed costs in 2010 for onshore wind farms typically ranged between $1800/kW and $2200/kW in most major markets. Wind turbines account for 64% to 84% of total installed costs onshore, with grid connection costs, construction costs, and other costs making up the balance. Off-shore wind farms are more expensive and cost $4000 to $4500/kW, with the wind turbines accounting for 44% to 50% of the total cost [13]. Modern wind turbines are designed to work for 120,000 hours throughout their estimated lifespan of 25 years. The life time of the wind turbine considered in this study was assumed to be 25 years. The estimated maintenance costs for modern machines are in the range of 1.5% to 2% of the original investment per annum [14]. Using these values, a 100 KW power plant capital cost will be $1.3 million and the expected O&M cost for the same power plant was $15,000 per year.

3.2.4. Photovoltaic Arrays

The Sunpower x21-335-BLK solar module was selected for the design which has a life time of 25 years with a 21% efficiency. The electrical characteristics of the Sunpower x21-335-BLK are given in **Table 3**. The assumed installation cost of the 150 KW PV array system was $5.6 million with operational and maintenance cost at 1% of total investment cost. The duration factor was 80% for a lifetime of 25 years.

3.2.5. Converter

A converter is a device that converts electric power from DC to AC in a process called inversion, and/or converting from AC to DC is a process called rectification. The converter size, which is a decision variable, refers to the inverter capacity, meaning the maximum amount of AC power that the device can produce by inverting DC power. The rectifier capacity, which is the maximum amount of DC power that the device can produce by rectifying AC power as a percentage of the inverter capacity, has been specified. The final physical properties of the converter are its inversion and rectification efficiencies, which were assumed to be constant. The inverter and rectifier efficiencies were assumed to be 90% and 85% for this study. The inverter capacity size was selected as 10 kW at a cost of $0.30 million and inverter lifetime of 15 years. Operating and maintenance cost

Table 3. Electrical characteristics of Sunpower x21-335-BLK solar module.

Maximum Power	335 W
Type of Cell	Polycrystalline Silicon
Cell Configuration	72 in Series
Open Circuit Voltage Voc	45.1 V
Maximum Power Voltage Vpm	35.2 V
Short Circuit Current Isc	8.94 A
Maximum Power Current Ipm	8.52 A
Module Efficiency	21%
Maximum System Voltage (DC)	1000 V
Dimensions	994 × 1971 × 46 mm

was assumed to be 1% of the inverter cost.

4. Results and Discussions

In this Section, the results of the designed wind-solar hybrid power generation system are presented and the conclusions from the findings are given.

4.1. Results Analysis

4.1.1. Simulation

HOMER simulates the operation of a system by making energy balance calculations in each hourly time step of the year. For each time step, HOMER compares the electric demand in that time step to the energy that the system can supply in that time step. Then, it calculates the flow of energy to and from each component of the system. HOMER performs these energy balance calculations for each system configurations that were considered. It then determines whether a configuration is feasible, *i.e.*, whether it can meet the electric demand under the specified conditions, and estimates the cost of installing and operating the system over the lifetime of the project. The number of installed 100 kW wind turbines was varied from 0 to 10 and the PV modules and converter sizes varied between 0 - 150 kW for the proposed system.

4.1.2. Optimization

After simulating all of the possible system configurations, HOMER displayed a list of configurations sorted by net present cost (NPC), *i.e.* lifecycle cost, which can be used to compare the different system design options. The NPC of a component is the net present value of all the costs of installing and operating that component over the project lifetime, minus the present value of all the revenues that it earns over the project lifetime. HOMER calculates the NPC of each component in the system, and of the system as a whole. Figure 6 shows the categorized

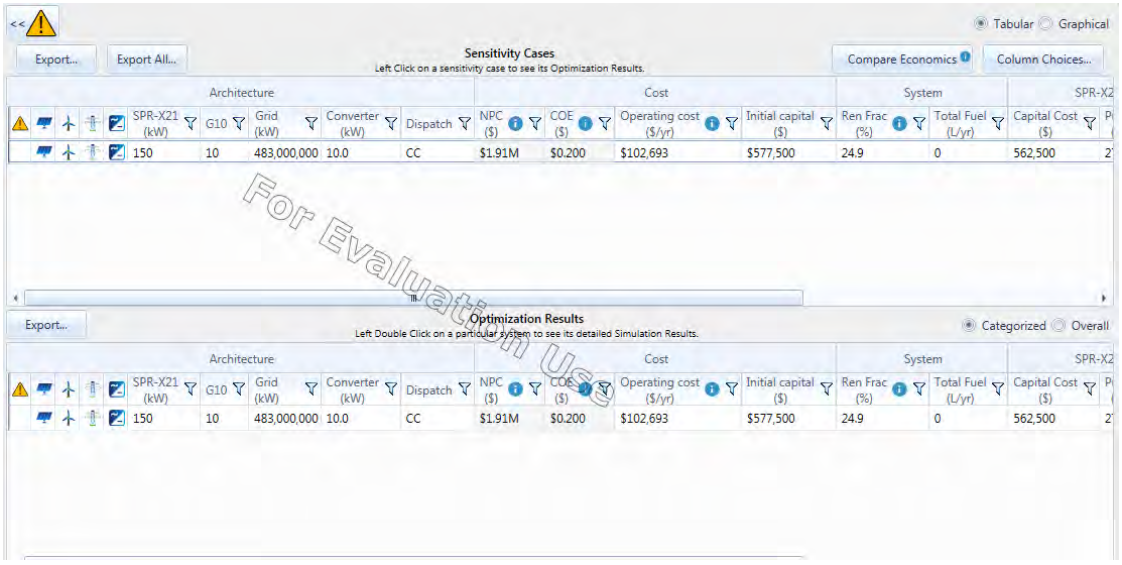

Figure 6. Categorized HOMER optimization results.

HOMER optimization results. In each category of a different design type it shows only the lowest NPC configuration. In Figure 7 the overall HOMER optimization results are presented.

Figure 7 shows that the 100 kW wind turbine and a 150 kW PV module with a 10 kW converter give the cheapest configuration. This configuration has a COE of 0.2 $/kWh and NPC value of $59,305,207. Figure 8 shows the monthly average power production of the selected hybrid system.

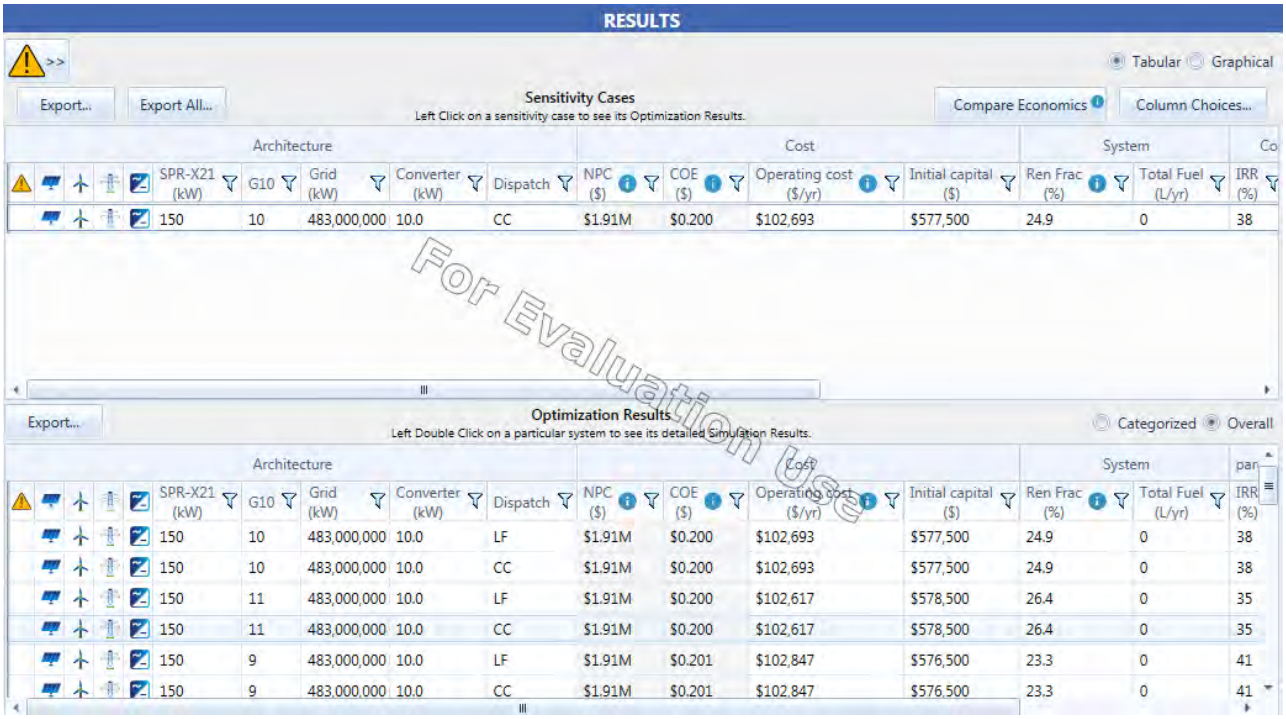

Figure 7. Overall HOMER optimization results.

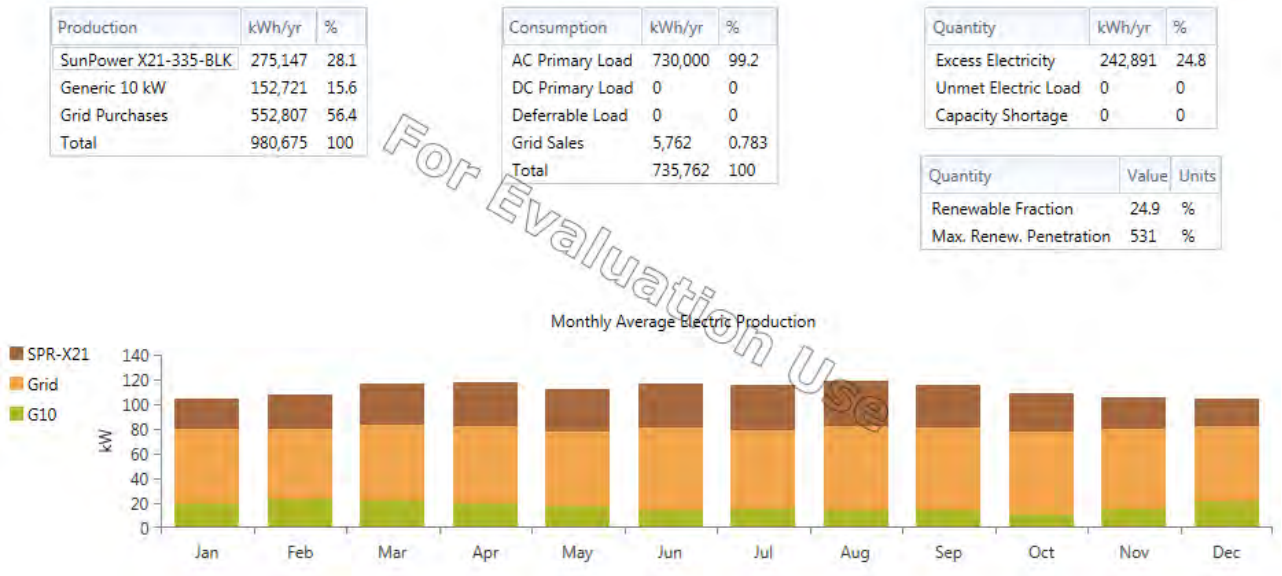

Figure 8. Monthly average power production of the wind-solar hybrid system.

The total annual power generation from the hybrid system was 0.427 GWh, where the solar contributed 0.27 GWh (28%) and 0.15 GWh (15%) was obtained from the wind. Annual generation details obtained from HOMER are given in Table 4.

Annual PV Output Variation and Wind Turbine Variation are shown in Figure 9 and Figure 10, respectively.

4.1.3. Financial Evaluation

The financial feasibility of the project was examined using the simple payback method, in which the payback period was the time it takes for the return on the investment to re-pay the sum of the original investment. The original investment in this context was the sum of all investments that are related to the purchasing and installation of wind-solar hybrid system. The return was the income generated

Table 4. Annual generation details of the proposed hybrid system.

Quantity	Units	PV Array	Wind Turbines
Rated capacity	Kw	150	100 (10 × 10)
Mean output	Kw	31.4	17.4
Maximum output	Kw	157	100
Total production	kWh/yr	275,147	152,721
Hours of operation	hr/yr	4357	6916
Capacity factor	%	20.9	17

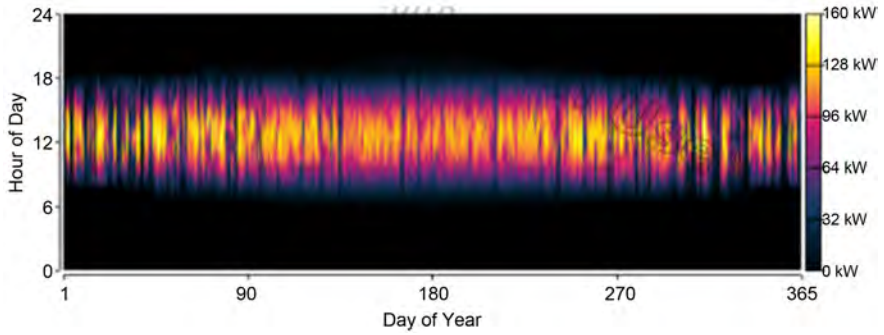

Figure 9. Annual PV output variation.

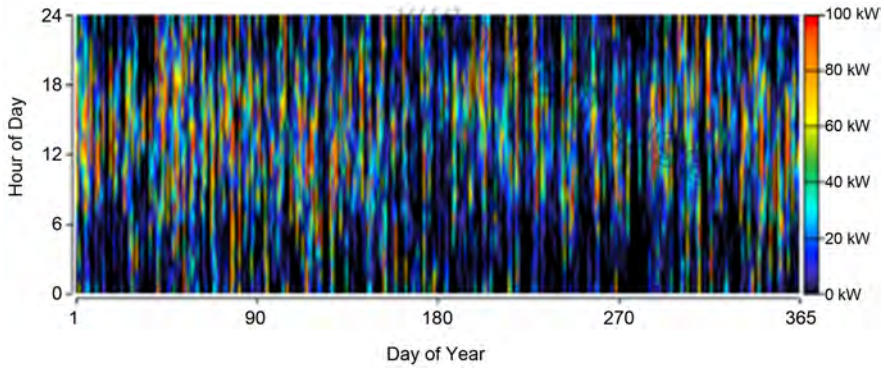

Figure 10. Annual wind turbine output variation.

by sale of electricity, reduced by the cost of operation and maintenance. Figure 11 shows the cost and income distributed over the lifetime of the project.

Total generation capacity of the design plant = 0.427 GWh/year.

Initial investment = $5.6 million.

Simple payback period = 2.6 years.

Internal Rate of Return (IRR) = 38.2%.

The hybrid model gave a simple recovery period of no more than 2.6 years. Given that the typical wind turbine and solar photovoltaic group has an economic life of up to 25 years, this indicates that an investment will certainly be profitable for the local conditions identified for the renewable energy resources and the very high costs of generating fossil fuel.

5. Environmental Impact

Wind or solar power cannot be the sole source of electricity in a stable base-load grid, but they can reduce the use of conventional energy sources. The environmental benefits of the wind-solar hybrid system in this study were assessed in terms of avoided emissions. Given that a conventional thermal power plant emits a certain amount of pollutant per kWh of generated electricity, the wind-solar hybrid system can be considered to cause an avoidance of emissions, since it generates the electricity with nearly zero pollutant emissions. Although there are many types of emissions related to electricity production, CO_2, sulfur dioxide and nitrogen oxides emissions were considered. CO_2 was the largest component of the emissions from a conventional electricity production plant and may be considered as the greatest environmental impact caused by the

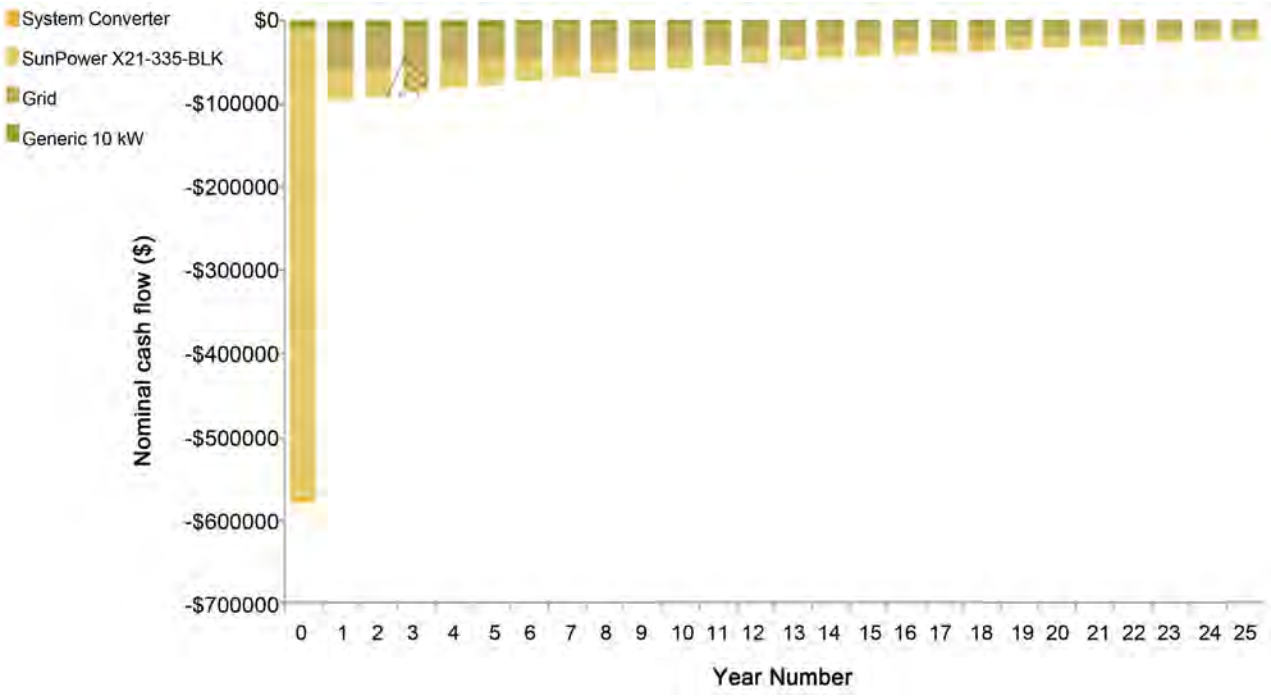

Figure 11. Cost and income distributed over the lifetime of the project.

power industry. The amount of CO_2 produced by conventional diesel fuel is 0.6 kg for 1 kWh. Hence, the reduction of CO_2 from energy saving of 0.427 GWh would be 331 tons/y, and 1.5 - 0.74 tons/y annually for sulfur dioxide and nitrogen oxides emissions.

6. Conclusion

There exists a worldwide concern regarding the energy security and sustainable development of energy across the globe. The role of renewable energy has therefore become more significant. The developed world is already on track for reducing the fossil fuel usage and developing the areas of renewable energy technologies. Through this study, an insight into the energy situation and renewable energy potential of Libya was given. It was identified that Libya has an economically feasible power generation potential of wind and solar energy. Using the HOMER simulation code, a grid-tied wind-solar hybrid power generation system was modeled for a selected location in the Al-Marj's area of Libya (MARJU), located on the coastal belt near Benghazi. Through the simulation process, the installation of ten 100 kW wind turbines and 150 kw solar PV arrays was identified as a most feasible economical design to supply average load connected to grid where payback period of the design was 2.6 years.

Conflicts of Interest

The authors declare no conflicts of interest regarding the publication of this paper.

References

[1] Mohamed, A. and Al-Habaibeh, H. (2013) An Investigation into the Current Utilization and Prospective of Renewable Energy Resources and Technologies in Libya. *Renewable Energy*, **50**, 732-740. https://doi.org/10.1016/j.renene.2012.07.038

[2] http://www.dlr.de/tt/en/desktopdefault.aspx/tabid-2885/4422_read-16596/

[3] Fesli, U., Bayir, R. and Özer, M. (2009) Design and Implementation of a Domestic Solar-Wind Hybrid Energy System. *Proceedings of the International Conference on Electrical and Electronics Engineering*, Bursa, Turkey, 5-8 November 2009, I-29-I-33.

[4] Amutha, W.M. and Rajini, V. (2015) Techno-Economic Evaluation of Various Hybrid Power Systems for Rural Telecom. Renewable and Sustainable Energy Reviews, **43**, 553-561. https://doi.org/10.1016/j.rser.2014.10.103

[5] Nafeh, A.E.S.A. (2011) Optimal Economical Sizing of a PV-Wind Hybrid Energy System Using Genetic Algorithm. *International Journal of Green Energy*, **8**, 25-43. https://doi.org/10.1080/15435075.2010.529407

[6] Dursun, B., Gokcol, C., Umut, I., Ucar, E. and Kocabey, S. (2013) Techno-Economic Evaluation of a Hybrid PV-Wind Power Generation System. *International Journal of Green Energy*, **10**, 117-136. https://doi.org/10.1080/15435075.2011.641192

[7] HOMER. http://homerenergy.com

[8] Ataei, A., Biglari, M., Nedaei, M., Assareh, E., Choi, J.K., Yoo, C. and Adaramola, M.S. (2015) Techno-Economic Feasibility Study of Autonomous Hybrid Wind and Solar Power Systems for Rural Areas in Iran, a Case Study in Moheydar Village. *En-*

vironmental Progress & Sustainable Energy, **34**, 1521-1527. https://doi.org/10.1002/ep.12121

[9] Shahinzadeh, H., Abadi, M.M.N., Hajahmadi, M. and Paknejad, A. (2013) Design and Economic Study for Use the Photovoltaic Systems for Electricity Supply in Isfahan Museum Park. *International Journal of Power Electronic and Drive Systems*, **3**, 83-94. https://doi.org/10.11591/ijpeds.v3i1.1797

[10] Fulzele, J.B. and Dutt, S. (2011) Optimium Planning of Hybrid Renewable Energy System Using HOMER. *International Journal of Electrical and Computer Engineering*, **2**, 68-74. https://doi.org/10.11591/ijece.v2i1.157

[11] NASA Surface Meteorology and Solar Energy. https://eosweb.larc.nasa.gov/sse/

[12] http://www.windustry.org/community-wind/toolbox/chapter-15-turbine-selection-andpurchase

[13] International Renewable Energy Agency (2012) Renewable Energy Technologies Cost analysis Series, Volume 1: Power Sector, Issue 5/5, Wind Power.

[14] http://www.windmeasurementinternational.com/wind-turbines/om-turbines.php

[15] GECOL. (2010) GECOL Annual Report 2010. General Electricity Company of Libya, Tripoli, Libya.

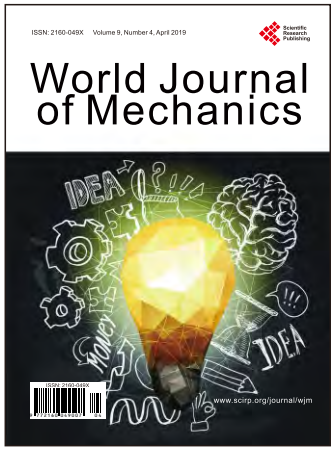

Call for Papers

World Journal of Mechanics (WJM)

ISSN 2160-049X (Print) ISSN 2160-0503 (Online)
http://www.scirp.org/journal/wjm

World Journal of Mechanics (WJM) is an international peer-reviewed journal dedicated to presenting the English original research studies, reviews in the general field of mechanics including the mechanics of solids, structures and fluids and their interaction.

Subject Coverage

This journal invites original research and review papers that address the following issues. Topics of interest include, but are not limited to:

- Applied Mathematics and Mechanics
- Biomechanics and Modeling in Mechanobiology
- Celestial Mechanics and Dynamical Astronomy
- Classical and Quantum Aspects of Mechanics
- Computational Mechanics
- Computer Methods in Applied Mechanics and Engineering
- Continuum Mechanics and Thermodynamics
- Damage Mechanics
- Dynamics and Vibration Control
- Elasticity and Plasticity
- Engineering Fracture Mechanics
- Environmental Fluid Mechanics
- Experimental Mechanics
- Fluid Mechanics and Aerodynamics
- Mathematical Fluid Mechanics
- Mathematics and Mechanics of Solids
- Mechanical Behavior of Biomedical Materials
- Mechanical Engineering Science
- Mechanical Systems and Signal Processing
- Mechanics & Astronomy
- Mechanics and Materials in Design
- Mechanics in Medicine and Biology
- Mechanics of Materials
- Mechanics of Time-Dependent Materials
- Microfluidics
- Micromechanics and Microengineering
- Multi-Scale Mechanics
- Nanomechanics
- Non-Linear Mechanics
- Non-Newtonian Fluid Mechanics
- Numerical and Analytical Methods in Geomechanics
- Probabilistic Engineering Mechanics
- Rock Mechanics and Mining Sciences
- Solid and Structural Mechanics
- Statistical Mechanics and Its Applications
- Terramechanics
- Theoretical and Applied Fracture Mechanics
- Thermophysics and Aeromechanics
- Thin Film Mechanics
- Viscoelasticity

We are also interested in short papers (letters) that clearly address a specific problem, and short survey or position papers that sketch the results or problems on a specific topic. Authors of selected short papers would be invited to write a regular paper on the same topic for future issues of World Journal of Mechanics.

Notes for Intending Authors

Submitted papers should not have been previously published nor be currently under consideration for publication elsewhere. Paper submission will be handled electronically through the website. All papers are refereed through a peer review process. For more details about the submissions, please access the website.

Website and E-Mail

http://www.scirp.org/journal/wjm E-mail: wjm@scirp.org

What is SCIRP?

Scientific Research Publishing (SCIRP) is one of the largest Open Access journal publishers. It is currently publishing more than 200 open access, online, peer-reviewed journals covering a wide range of academic disciplines. SCIRP serves the worldwide academic communities and contributes to the progress and application of science with its publication.

What is Open Access?

All original research papers published by SCIRP are made freely and permanently accessible online immediately upon publication. To be able to provide open access journals, SCIRP defrays operation costs from authors and subscription charges only for its printed version. Open access publishing allows an immediate, worldwide, barrier-free, open access to the full text of research papers, which is in the best interests of the scientific community.

- High visibility for maximum global exposure with open access publishing model
- Rigorous peer review of research papers
- Prompt faster publication with less cost
- Guaranteed targeted, multidisciplinary audience

Scientific Research Publishing

Website: http://www.scirp.org

Subscription: sub@scirp.org

Advertisement: service@scirp.org